28

Photovoltaic Effect in Ferroelectric $LiNbO_3$ Single Crystal

Zhiqing Lu, Kun Zhao and Xiaoming Li
Laboratory of Optic Sensing and Detecting Technology, College of Science
People's Republic of China

1. Introduction

Lithium niobate ($LiNbO_3$) is a human-made dielectric material and was first discovered to be ferroelectric in 1949. Properties and applications of $LiNbO_3$ have been widely studied, resulted in several thousands of papers on this material, since the crystal was successfully grown using the Czochralski method by Ballman in 1965 (Kong et al., 2005). It has been extensively researched for its excellent ferroelectric, piezoelectric, dielectric, pyroelectric, electric-optical and nonlinear optical properties (Wang et al., 2008; Chen et al., 2007; Sarkisov et al., 2000). Now $LiNbO_3$ is a very significant material for optical applications, such as acoustic wave transducers, acoustic delay lines, acoustic filters, optical amplitude modulators, optical phase modulators, second-harmonic generators, Q-switches, beam deflectors, dielectric waveguides, memory elements, holographic data processing devices, and others (Kim et al., 2001; Zhen et al., 2003; Pham et al., 2005; Liu et al., 2002; Zhou et al., 2006).

$LiNbO_3$ is a ferroelectric material which has the highest Curie temperature of about 1210 °C up to now and the largest spontaneous polarization of about 0.70 C/m^2 at room temperature. $LiNbO_3$ single crystals exhibit paraelectric phases above the Curie temperature and ferroelectric phases below the Curie temperature (Karapetyan et al., 2006; Bermúdez et al., 1996). Ferroelectric $LiNbO_3$ crystal is a member of the trigonal crystal system, exhibiting three-fold rotation symmetry about its c axis. Its structure consists of planar sheets of oxygen atoms in a distorted hexagonal close-packed configuration. The octahedral interstices in this structure are one-third filled by lithium atoms, one-third by niobium atoms, and one-third vacant. In the paraelectric phase the Li atoms and the Nb atoms are centered in an oxygen layer and an oxygen octahedral, making the paralelctric phase non-polar. But in ferroelectric phase the Li atoms and the Nb atoms shifted into new positions along the c axis by the elastric forces of the crystal, making the $LiNbO_3$ crystal exhibiting spontaneous polarization (Bergman et al., 1968).

Many methods were reported to determine the +c axis of ferroelectric $LiNbO_3$ single crystal. A standard method is to compress the crystal in the c axis direction. The +c axis is defined as being directed out of the c face that becomes negative upon compression. This can be understood that the Li and Nb ions move closer to their centered positions upon compression, leaving excess negative compensation charges on the +c face, causing the +c face to become negative. Anther method to identify the +c face and –c face of the crystal is an etching technique with HF solution. The etching speed on the –c face is faster than on the +c face (Beghoul et al., 2008; Bourim et al., 2006). Other methods to determine the +c axis

were also reported such as to cool the crystal, observation of the terraces on a cleavage plane, x-ray diffraction techniques (Boyd et al.,1964; Kaminow et al., 1980).

In the past few years, various types of photodetectors were proposed, such as photoconductor, Schottky barrier detector, p-i-n junction photodiode, and heterogeneity junction (Wang et al., 2007; Jin et al., 2007). Photovoltaic effect plays an important role in the investigation of these photodetectors. Photovoltaic effects in $LiNbO_3$ crystals were observed by Chen in 1969 (Chen, 1969). Then $LiNbO_3$ was found to be in response to ultraviolet, visible, and infrared radiation of laser (Dai et al., 2005). $LiNbO_3$ is a promising material for photodetector because of its high responsibility, good dielectric properties, and low cost. For example, ultraviolet photodetectors have attracted a strong interest owing to their broad potential applications in the fields of automatization, short-range communications security, biological researches, and military services. The band gap of $LiNbO_3$ single crystal is ~ 4 eV, which can be suggested as a promising material for UV photodetector since the present ultraviolet photodetectors based on various wide band gap semiconductors, such as III–V nitrides, silicon carbide, zincoxide, and diamond, require a complicated fabrication process and high-cost manufacturing (Razeghi & Rogalski, 1996; Topic et al., 2001; Tomm et al., 2000; Spaziani et al., 2003). In this chapter, photovoltaic effect in pure congruent $LiNbO_3$ single crystals will be introduced, including vertical photovoltaic effect, lateral photovoltaic effect and photovoltaic effects in miscut $LiNbO_3$ single crystals (Lu et al., 2009; Li et al.,2010).

2. Photovoltaic effects in $LiNbO_3$ single crystal

2.1 Vertical photovoltaic effects

Commercial optical grade z-cut $LiNbO_3$ single crystal was used in the experiment, which was double polished with a dimension of 5×5×0.5 (mm) in the a, b, and c directions, respectively. The two silver paste electrodes were placed on the opposite two surfaces of the crystal respectively. An actively/passively mode locked Nd:yttrium-aluminum-garnet (Nd:YAG) laser (with pulse duration of 25 ps, repetition rate of 10 Hz) was used to irradiate the sample at the wavelengths of 1064, 532, and 355 nm at room temperature. The laser beam was directed onto the sample near to the electrode and passed through the crystal along the c axis, as shown in the inset in Fig.1. The diameter of the spot was 2 mm. The open circuit photovoltage were measured and recorded by a digital storage oscilloscope. Figure 1 presents the typical ultrafast photovoltaic signals observed under the pulsed laser of three different wavelengths. The laser pulse energy of 355, 532 and 1064 nm is 0.56, 0.60 and 0.58 mJ respectively .We can see that the response time is about 2 ns and the full width at half maximum (FWHM) is about 1.8 ns.

All the photovoltages measured by the oscilloscope were negative whether the laser pulse irradiated on the top surface or on the bottom surface of the crystal, shown in Fig.1. It has been known that the ferroelectric $LiNbO_3$ exhibits spontaneous polarization below its Curie temperatures, which direction is from –c face to +c face of the crystal (Wemple et al., 1968). So there is a built-in electric field in $LiNbO_3$ crystal in the direction from the positive end of spontaneous polarization to the negative end, antiparallel to the spontaneous polarization. Here we identified the –c face and +c face using an etching technique with HF solution of 40%. When the laser spot directed on the crystal, photo-excited electrons drifted toward the positive end of spontaneous polarization under the influence of the internal electric field, undergoing the course of excited-captured-reexcited-recaptured before they eventually

drifted to the +c face. So we always get a negative signal on the oscilloscope whether the laser irradiated on the +c face or on the –c face.

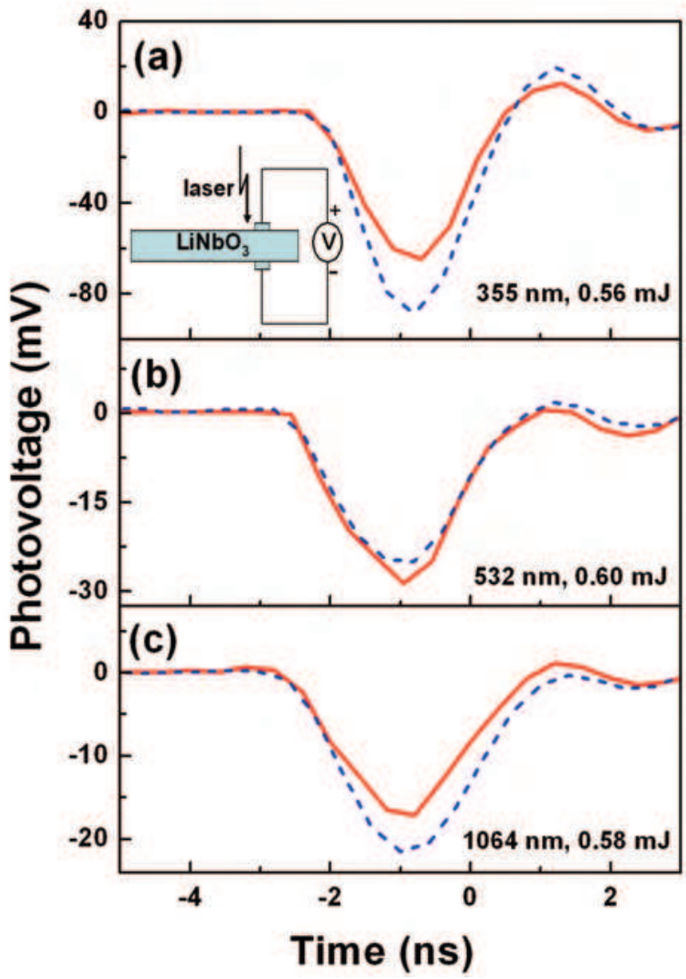

Fig. 1. Typical ultrafast photovoltage with time when the sample irradiated by pulsed laser of three different wavelengths. The solid line is the signal when irradiated on the +c face of the crystal and the short dash line is on the –c face. All the signals measured are negative.

The peak voltage values of open circuit verse the pulse energy has been also measured under the irradiation of the three different wavelengths. The results are summarized in Fig.2. We can see that the photovoltages under the three wavelengths increased linearly with the incident energy of each laser pulse.

The photovoltage V that appears in the crystal is (Feng et al., 1990)

$$V = \frac{J}{\sigma_d + \sigma_{ph}} l \tag{1}$$

where J is the photovoltaic current, σ_d and σ_{ph} are dark conductivity and photoconductivity of the crystal, respectively, and l is the distance between the electrodes. Since σ_d ($<10^{-15}\Omega^{-1}cm^{-1}$) is much smaller than σ_{ph}, we can neglect it.

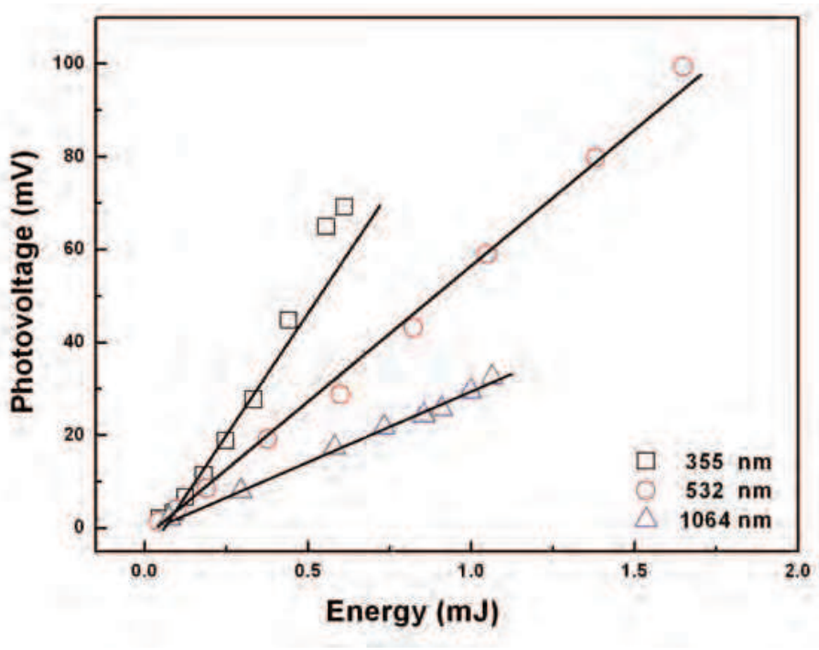

Fig. 2. The peak open-circuit photovoltage as a function of the energy of pulsed laser. The photovoltage is proportional to the intensity of incident laser of 355, 532 and 1064 nm, respectively.

The photovoltaic current of $LiNbO_3$ crystal is given by (Glass et al., 1974)

$$J = \kappa\alpha I + \sigma_{ph}E + eD\frac{dn}{dz} \tag{2}$$

where κ is the glass coefficient, α is the absorption coefficient, I is the intensity of the irradiated laser beam, E is the total electric field in the crystal, D is the diffusion coefficient, and n is the carrier concentration. The first term represents the photovoltaic current, the second term represents the drift current, and the third term represents the non-uniform laser irradiation in the sample.

The photoconductivity is given by (Nakamura et al., 2008)

$$\sigma_{\mathrm{ph}} = \frac{\alpha I}{\mathrm{h}\nu}\tau e\mu \tag{3}$$

where τ is the lifetime of an excited carrier in the conduction band, μ is the mobility, and $h\nu$ is the photon energy.

The carrier concentration n should be proportional to the intensity of the laser due to the photoelectric effect. So the photovoltage V is proportional to the intensity of incident laser I, as shown in Fig.2.

Continuous-wave (CW) laser of 532 and 1064 nm were also used to irradiate on the sample. Negative photovoltage signal was also observed in the experiment, as shown in Fig.3. This is in agreement with the results of the experiments above using pulsed lasers in Fig.1. The reason is the existence of the spontaneous polarization and the internal electric field in the crystal. When the power of the incident laser was changed from 0.6 to 60.4 mW, we found that the peak photovoltages also increased linearly, as shown in Fig.4.

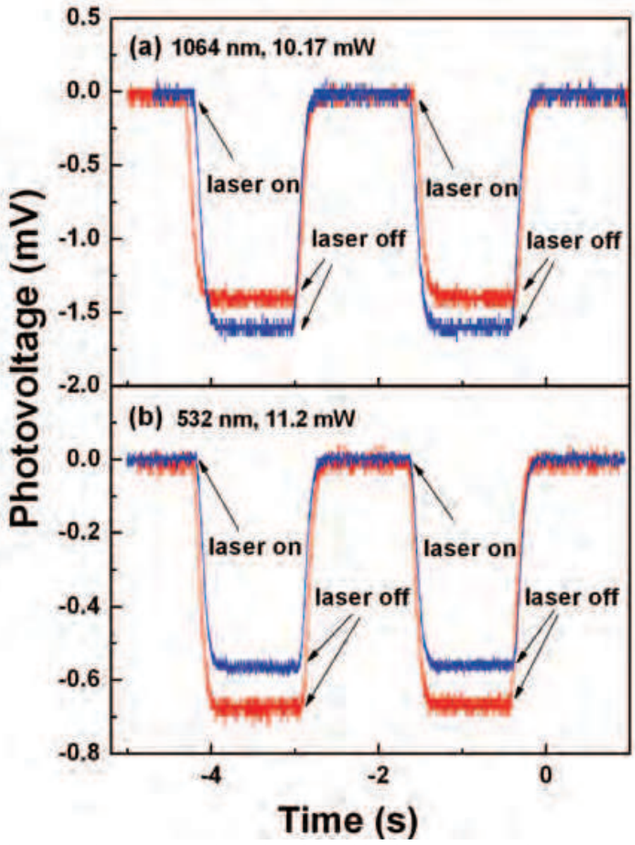

Fig. 3. The negative photovoltages under the irradiation of continuous-wave laser of 532 and 1064 nm.

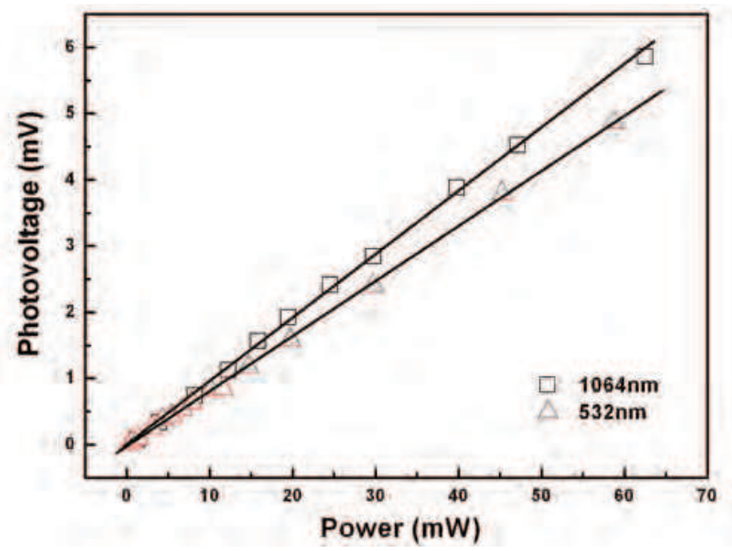

Fig. 4. The open-circuit photovoltages increased linearly with the intensity of the CW laser.

Defects in $LiNbO_3$ crystal are the main reason of the photovoltaic effect and the charge transport. There is at least about 1 mol % of intrinsic defects such as bipolarons and small

polarons in pure congruent $LiNbO_3$ crystal (Schirmer et al., 2005). The absorption spectra of $LiNbO_3$ (Fig.5) shows that the absorption peak of the sample is about at 310 nm, and there is a common absorption peak of bipolarons and small polarons at 628 nm. So the transition and migration of the electrons in $LiNbO_3$ crystal is mainly between the defects and the conduction band.

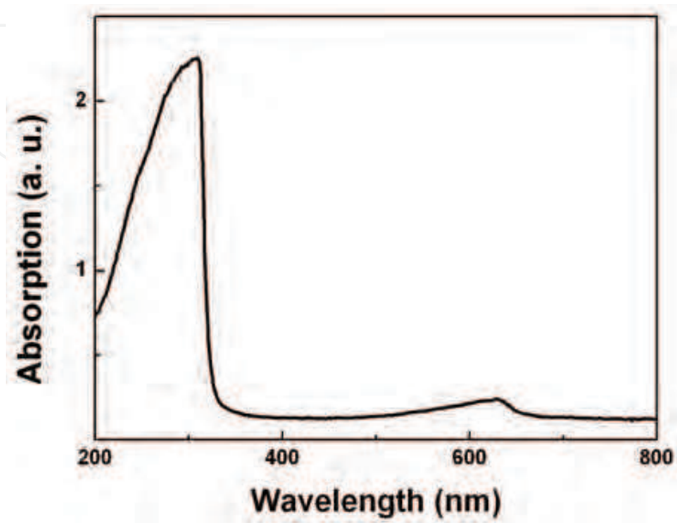

Fig. 5. The absorption spectra of $LiNbO_3$ which shows two absorption peaks of the sample that one is for band to band absorption and another is the common absorption peak of bipolarons and small polarons.

On the basis of two-center model, for pure $LiNbO_3$, the deep center is dominated by bipolarons and the shallow center is governed by the small polarons. By laser pulses these bipolarons can be dissociated at room temperature and released photo-excited electrons to the conduction band. But the amount of the shallow center is very small in pure $LiNbO_3$. The energy between the deep center and the conduction band is about 2.0~2.5 eV. The photon energy of 355 nm is 3.5 eV. So when the sample was irradiated by the laser of 355 nm, a large amount of electrons in deep center can be excited into the conduction band. The photon energy of 532 nm is 2.3 eV, which is near to the energy between the deep center and the conduction band, so it can excited part of electrons in deep center. Therefore, the peak value of photovoltage of 355 nm is larger than that of 532 nm, as shown in Fig.2. The photon energy of 1064 nm is 1.2 eV, which can not excite the electrons in deep center. But the deep center can be dissociated not only by illumination but also heating. The temperature of the crystal increased during the irradiation of 1064 nm laser in the experiment, and the deep center is dissociated and released electrons. With the increase of the intensity of the incident laser, the transition between the deep center and the shallow center should be taken into account, for the dissociated energy of bipolarons is about 0.27 eV (Kong et al., 2005) .

2.2 Lateral photovoltaic effects

To investigate the lateral photovoltage in $LiNbO_3$ single crystal, two silver paste electrodes were separated about 1.5 mm on the surface perpendicular to the c axis. The laser beam passed through the crystal along the c axis and irradiated normally at the back of one electrode, as shown in Fig. 6.

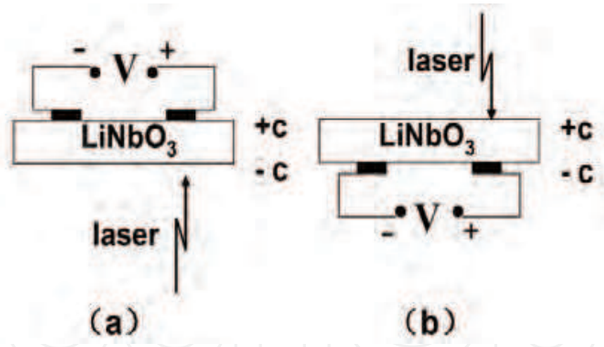

Fig. 6. Schematic of measurement for sample irradiated by laser through (a) −c face (mode 1) and (b) +c face (mode 2).

Typical ultrafast signals can be observed as shown in Fig. 7, with the rise time of about 1.5 ns and the FWHM of 1−2 ns. For mode 1, the signals were negative and positive when the laser pulse irradiated the positive and negative electrodes, respectively (Fig. 6(a)). While the reverse signals were recorded for mode 2 (Fig. 6(b)).

Due to inhomogeneous illumination in $LiNbO_3$ crystal, the concentration of photoelectrons is larger in the illumination region than in the dark region. And the photoelectrons will drift toward the +c face of the crystal because of the existence of a permanent electric field in the direction from −c to +c faces, then diffuse toward another electrode. Thus we can get the negative (positive) signals when the sample is irradiated at the back of positive electrode for mode 1 (mode 2). The same results can be also obtained when the CW laser is used to irradiate the crystal, as shown in Fig. 8. The dependence of the peak open-circuit photovoltages on the incident light intensity is studied experimentally. The results are summarized in Fig. 9. We can see that the photovoltages increase linearly with the laser intensity, which can be well explained by the photovoltaic effects in $LiNbO_3$ crystal.

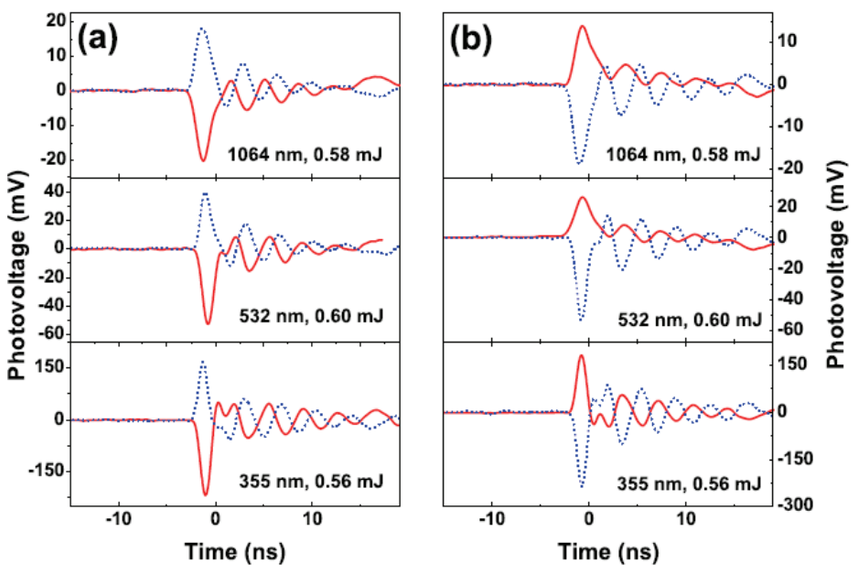

Fig. 7. Typical ultrafast photovoltages recorded for (a) mode 1 and (b) mode 2. Solid and short dot lines are for the signals when the laser pulse irradiates the positive and negative electrodes, respectively.

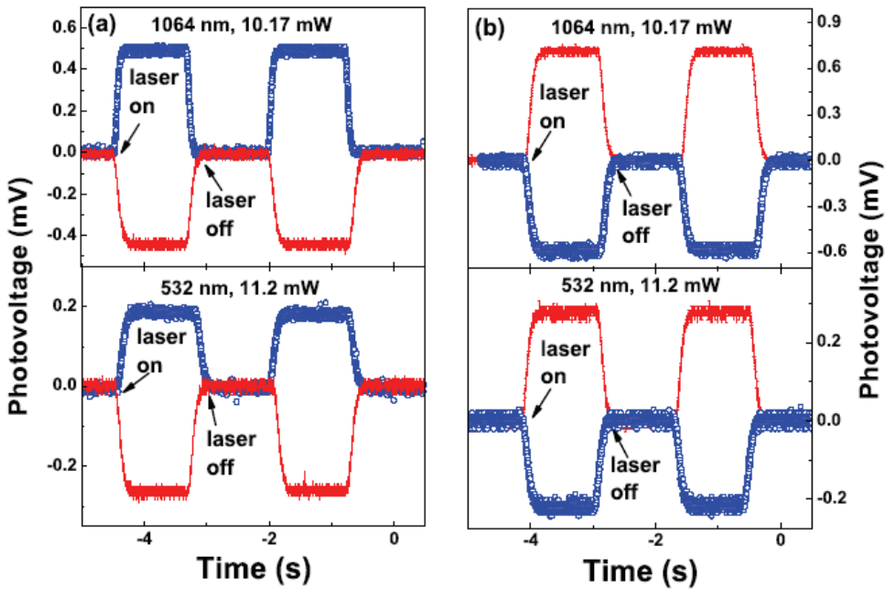

Fig. 8. Photovoltages for (a) mode 1 and (b) mode 2 under the irradiation of CW laser of 532 and 1064 nm. Solid line and open circle point are for the signals when the laser pulse irradiates the positive and negative electrodes, respectively.

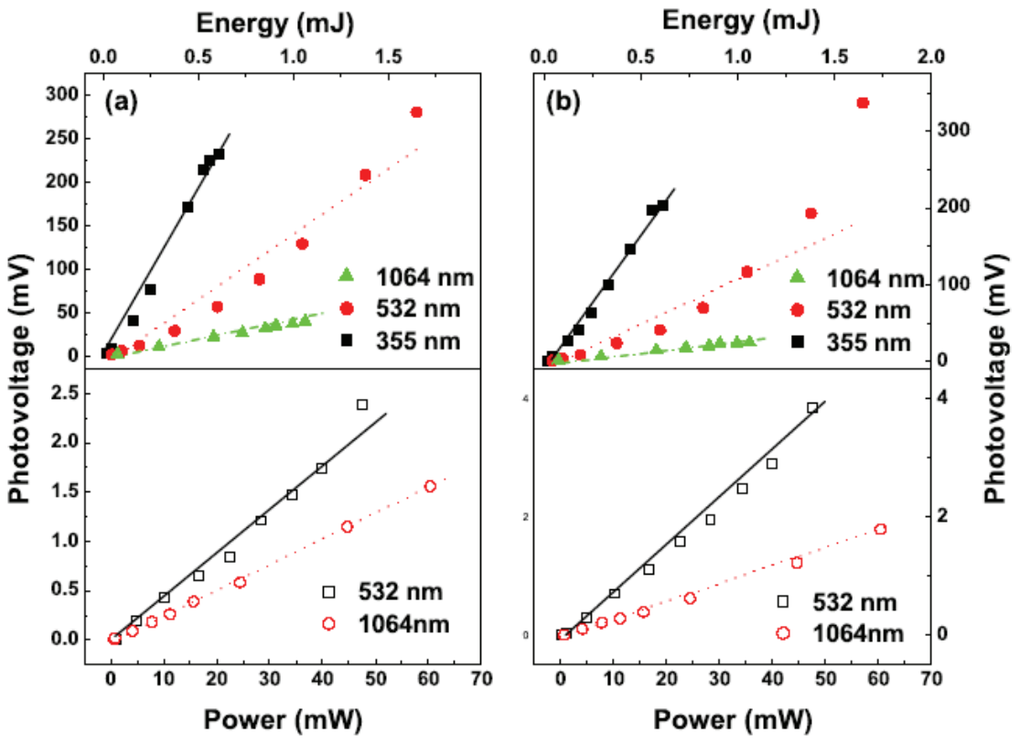

Fig. 9. Peak open-circuit photovoltages as functions of pulsed laser energy (solid point) and CW laser power densities (open point) for (a) mode 1 and (b) mode 2.

2.3 Photovoltaic effects in miscut $LiNbO_3$ single crystals

A single polished commercial $LiNbO_3$ single crystal with *c*-axis oriented is used for the photovoltaic studies. The sample geometry is 5×5 mm² with the thickness of 0.5 mm. The crystalline orientation is 10° miscut from the exact (001) orientation, which is characterized by x-ray diffraction with the usual θ-2θ scan using Cu Ka_1 and Ka_2 radiations. As shown in Fig. 10, the offset point is set as ω=a or 45°-a to satisfy Braggs diffraction, where α is the miscut angle. The two peaks arise from the (006) and (0012) plane of $LiNbO_3$ and are clearly apart for Ka_1 and Ka_2 radiations. The inset of Fig. 10 shows the UV–visible absorption spectrum of $LiNbO_3$ crystals as a function of the wavelength. The sharp absorption edge is about 310 nm, corresponding to the optical band gap of $LiNbO_3$ and indicating that UV light, e.g. 248 nm laser, can generate electron–hole carriers in $LiNbO_3$ crystals.

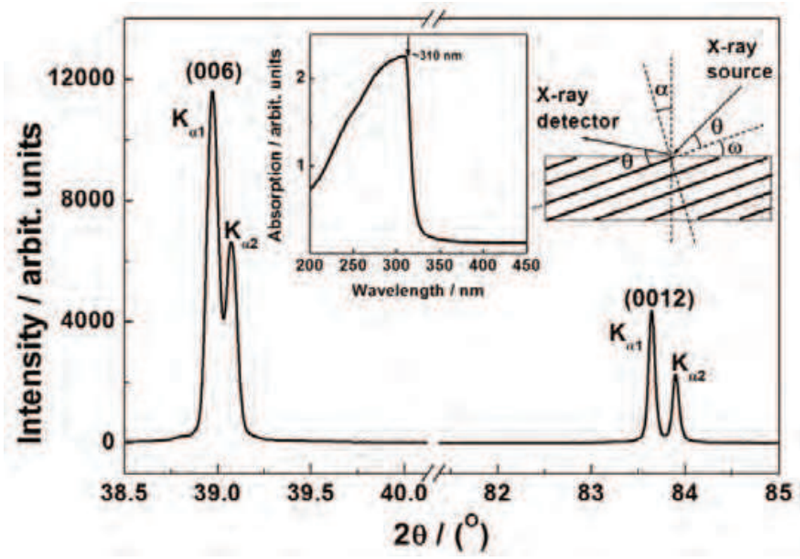

Fig. 10. The x-ray diffraction pattern of a miscut $LiNbO_3$ single crystal. The left inset shows the absorption spectrum of $LiNbO_3$ single crystal. The right inset shows the configuration of θ-2θ scan, where a is the miscut angle and ω the offset point.

The photovoltaic properties are investigated under the illuminations of a KrF pulsed laser with the wavelength of 248 nm with 20 ns duration at a 10 Hz repetition. In order to study the influence of the thickness on the photovoltaic effect, the samples are polished mechanically into seven different thicknesses, which are 0.49, 0.45, 0.38, 0.28, 0.22, 0.17 and 0.09 mm, respectively. Before the photovoltaic measurements, the sample is cleaned by using an ultrasonic cleaner in alcohol and acetone under routine cleaning process. Two colloidal silver electrodes of about 1×5 mm² area, separated by 3 mm, are prepared on the mirror polished surface of the $LiNbO_3$ single crystal and the opposite surface is exposed wholly to the laser irradiation, as shown in the inset of Fig. 11. The photovoltaic signals are recorded by using a sampling oscilloscope terminating into 50 Ω at room temperature. All the measurements are carried out in the room temperature without any applied bias.

Typical voltage transients of the $LiNbO_3$ single crystal of different thicknesses to a pulsed laser illumination are presented in Fig. 11. The peak photovoltage as a function of the sample thicknesses is shown in Fig. 12, and the energies on the sample are 15.2 and 19.4 mJ,

respectively. With the decrease of the crystal thickness from 0.49 to 0.09 mm, the peak photovoltage increases rapidly at first and then descendes. The maximum peak photovoltage occurs at the thickness of 0.38 mm and reaches 35.6 and 31.1 mV for 19.4 and 15.2 mJ, with the corresponding photovoltaic sensitivities of 1.83 and 2.04 mV/mJ, which is several times larger than that at 0.49 and 0.09 mm. In addition, the peak photovoltage is found to depend linearly on the on-sample energy from 13.5 to 20.9 mJ for selected crystal thicknesses of 0.22 and 0.09 mm, respectively, as shown in Fig. 13.

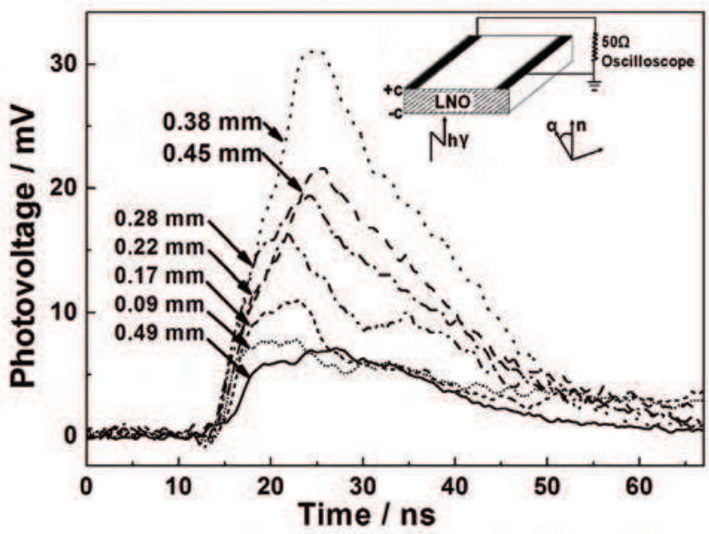

Fig. 11. The photovoltaic pulses for miscut $LiNbO_3$ single crystal under the illumination of a 248 nm laser for seven different thicknesses recorded by an oscilloscope with an input impedance of 50 Ω at room temperature without any applied bias. The on-sample energy was 15.2 mJ. The inset displays the schematic circuit of the measurement.

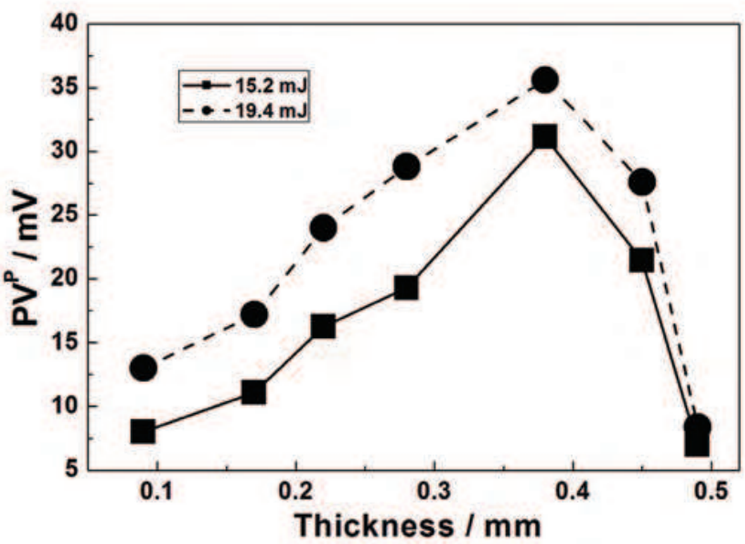

Fig. 12. The peak photovoltage dependence of the miscut $LiNbO_3$ single crystal thickness.

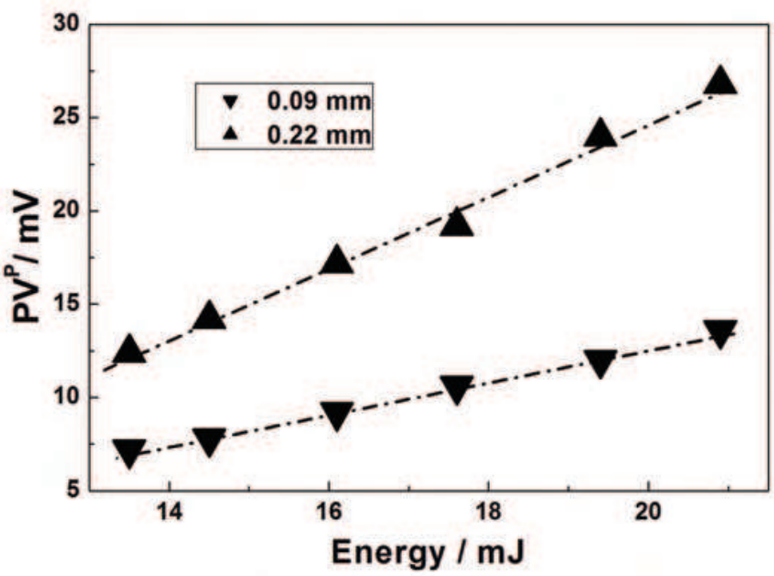

Fig. 13. The peak photovoltage of the miscut $LiNbO_3$ single crystal as a function of on-sample energy.

Figure 14 shows the 10%–90% rise time and FWHM as functions of the sample thickness for the on sample-energy of 15.2 and 19.4 mJ, respectively. With the decrease of sample thickness, the carriers reaches the two colloidal electrodes faster for thinner sample so that faster photovoltaic response can be observed. The rise time descends obviously from 11.83 ns at 0.49 mm to 3.946 ns at 0.09 mm, suggesting that decreasing the sample thickness is a useful way to obtain faster response detection. Since the miscut $LiNbO_3$ single crystal

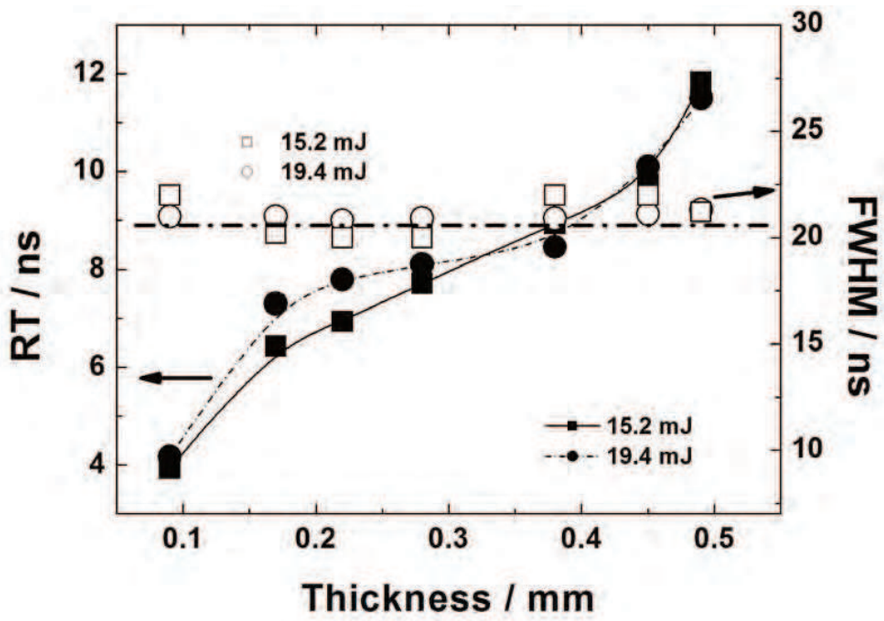

Fig. 14. The rise time and FWHM as functions of the sample thickness.

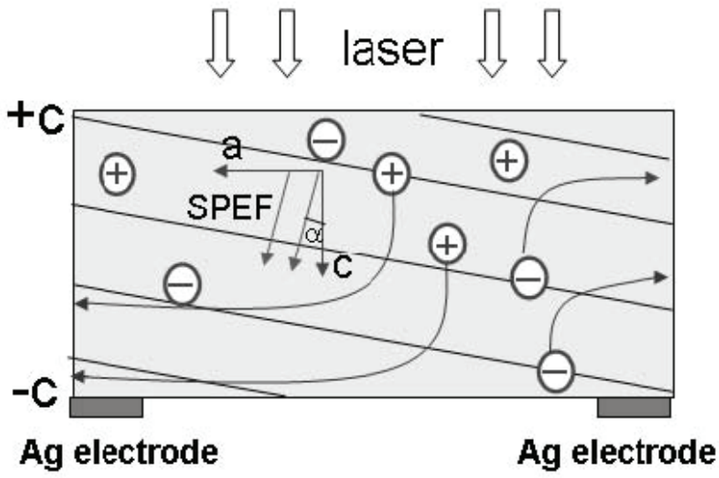

Fig. 15. The schematic diagram of the transporting photogenerated carriers, indicating that the carriers were separated and assembled at the two Ag electrodes by the SPEF.

exhibits an optical response time of ~ns, it can be applied to detect the present laser pulse, which is further confirmed in Fig. 14, where the FWHM is independent of crystal thickness and almost keeps a constant of ~20 ns in accord with the 248 nm laser duration.

It is well known that pure congruent $LiNbO_3$ is a spontaneous polarisation crystal and there exists a spontaneous polarisation electric field (SPEF) along the *c* axis. In the experiment, the crystalline orientation is 10° miscut from the exact (001) orientation, so is SPEF as shown in Fig. 15 Under the 248 nm laser irradiation, photo-induced carriers are separated and assembled at the two electrodes by the SPEF. Only those carriers reaching to the electrodes in the back can be collected and give rise to photovoltaic signals. With decrease of crystal thickness the amount of carriers collected by electrodes in the back increases due to lower loss, which is resulted from the shorter transport distances as well as less traps and recombination in thinner samples. Thus the signals for thinner samples are much larger than that for thicker samples. On the other hand, the decrease of thickness also leads to decrease of autologous carriers in $LiNbO_3$ single crystals, which limits the amount of carriers collected by electrodes. The competition between the two above factors results into a maximum photovoltaic signal at an optimum thickness at 0.38 mm.

3. Conclusion

The characteristics of the photovoltaic effect in $LiNbO_3$ single crystals were presented in detail in this chapter. Vertical and lateral photovoltaic effects in pure congruent $LiNbO_3$ crystals were observed by using pulsed and continuous wave lasers with inhomogeneous irradiation, respectively. The typical ultrafast response time and FWHM were about 2ns for the open-circuit photovoltaic pulse, indicating the potential applications of $LiNbO_3$ single crystal as photoelectronic detector. The thickness dependence of the photovoltaic effect in miscut $LiNbO_3$ single crystal was also investigated. With the decrease of the crystal thickness, the photovoltaic response time decreased monotonically, the photovoltaic sensitivity is improved rapidly at first, and then decreases. The experimental results show that decreasing the crystal thickness is an effective method for obtaining faster response time and improving the photovoltaic sensitivity in single crystals.

4. Acknowledge

This work was supported by the Program for NCET, NSFC, RFDP, Beijing Natural Science Foundation, Foresight Fund Program from China University of Petroleum (Beijing).

5. References

Kong Y. F.; Xu J. J.; Zhang G. Y.; Liu S. M. & Lu Y. (2005), *Multifunctional photoelectric material: $LiNbO_3$ crystals*. Science Press, ISBN 7-03-013660-8, Beijing

Wang, K.; Li, J. F. & Liu, N. (2008). Piezoelectric properties of low-temperature sintered Li-modified (Na, K)NbO_3 lead-free ceramics. *Appl. Phys. Lett.*, 93, 092904

Chen, J.; Li, Y. D.; Lu, W. Q.; Qi, J. W.; Cui, G. X.; Liu, H. B.; Xu, J. J. & Sun, Q. (2007). Observation of surface-plasmon-polariton transmission through a silver film sputtered on a photorefractive substrate. *J. Appl. Phys.*, 102, 113109

Sarkisov, S. S.; Curley,M. J.; Williams,E. K.; Ila,D.; Svetchnikov,V. L.; Zandbergen,H. W.; Zykov, G. A.; Banks,C.; Wang, J. C.; Poker, D. B. & Hensley, D. K. (2000). Nonlinear optical waveguides produced by MeV ion implantation in $LiNbO_3$. *Nuclear Instruments and Methods in Physics Research Section B: Beam Interactions with Materials and Atoms*, 166-167, 750-757

Kim, R. H.; Park, H. H. & Joo, G. T. (2001). The growth of $LiNbO_3$ (006) on MgO (001) and $LiTaO_3$ (012) substrates by sol-gel procedure. *Appl. Surf. Sci.*, 169-170, 564–569

Zhen, X. H.; Zhang, X. J.; Zhao, L. C. & Xu, Y. H. (2003). Growth and optical properties of In:Nd:$LiNbO_3$ crystals. *Solid State Commun.s,* 126, 203-206

Pham, V. T.; Lee, S. K.; Trinh, M. T.; Lim, K. S.; Hamilton, D.S. & Polgár, K. (2005). Nonvolatile two-color holographic recording in Tm-doped near-stoichiometric $LiNbO_3$. *Opt. Commun.s*, 248, 89-96

Liu, Y.; Kitamura, K.; Takekawa, S.; Ravi, G. & Nakamura, M. (2002). Nonvolatile two-color holography in Mn-doped near-stoichiometric lithium niobate. *Appl. Phys. Lett.*, 81, 2686-2688

Zhou, Q. F.; Cannata, J. & Shung, K. K. (2006). Design and modeling of inversion layer ultrasonic transducers using $LiNbO_3$ single crystal . *Ultrasonics*, 44, e607-e611

Karapetyan, K. G.; Kteyan,A. A. & Vardanyan, R. A. (2006) Thermal reduction effect on Curie temperature of $LiNbO_3$ ferroelectrics. *Solid State Commun.*, 140, 474-476

Bermúdez, V.; Dutta, P. S.; Serrano, M. D. & Diéguez, E. (1996). In situ poling of $LiNbO_3$ bulk crystal below the Curie temperature by application of electric field after growth. *J. Crystal Growth*, 169, 409-412

Bergman, J. G.; Askin, A.; Ballman, A. A.; Dziedzic, J. M.; Levinstein, H. J. & Smith, R. G. (1968). Curie temperature, birefringence, and irefringence, and phase-matching temperature variations in $LiNbO_3$ as a function of melt stoichiometry. *Appl. Phys. Lett.*, 12, 92-95

Beghoul, M. R.; Boudrioua, A.; Kremer, R.; Fontana, M. D.; Fougere, B.; Darraud, C.; Vareille, J. C. & Moretti, P. (2008). Micro-Raman spectroscopy investigation of the electron beam irradiation of $LiNbO_3$ surface for 2D photonic band gap grating inscription. *Opt. Mater.*, 31, 136-142

Bourim, E. M.; Moon, C. W.; Lee, S. W. & Yoo, I. K. (2006). Investigation of pyroelectric electron emission from monodomain lithium niobate single crystals. *Physica B*, 383,171-182

Boyd, G. D.; Miller, R. C.; Nassau, K.; Bond, W. L. & Savage, A. (1964). $LiNbO_3$: an efficient phase matchable nonlinear optical material. *Appl. Phys. Lett.*, 5, 234-236

Kaminow, I. P.; Turner, E. H.; Barns, R. L. & Bernstein, J. L. (1980). Crystallographic and electro-optic properties of cleaved $LiNbO_3$. *J. Appl. Phys.*, 51, 4379-4384

Wang, Q.; Lu, J. H.; Xiong, D. P.; Zhou, J.; Huang, H.; Miao, A.; Cai, S. W.; Huang, Y. Q. & Ren, X. M. (2007). Metamorphic $In_{0.53}Ga_{0.47}As$ p-i-n photodetector grown on GaAs substrates by low-pressure MOCVD. *Chin. Opt. Lett.* 5, 358-360

Jin, K. J.; Zhao, K.; Lu, H. B.; Liao, L. & Yang, G. Z. (2007). Dember effect induced photovoltage in perovskite *p-n* heterojunctions. *Appl. Phys. Lett.* 91, 081906

Chen, F. S. (1969). Optically Induced Change of Refractive Indices in $LiNbO_3$ and $LiTaO_3$. *J. Appl. Phys.*, 40, 3389-3397

Dai, C.; Liu, L. R,; Liu, D. A. & Zhou, Y. (2005). Refractive-index change and sensitivity improvement in holographic recording in $LiNbO_3$:Ce:Cu crystals with green light. *Chin. Opt. Lett.* 3, 507-510

Razeghi, M. & Rogalski, A. (1996). Semiconductor ultraviolet detectors. *J. Appl. Phys.*, 79, 7433-7474

Topic, M.; Stiebig, H.; Krause, M. & Wagner, H. (2001). Adjustable ultraviolet-sensitive detectors based on amorphous silicon. *Appl. Phys. Lett.*, 78, 2387-2390

Tomm, J. W.; Ullrich, B.; Qiu X. G.; Segawa, Y.; Ohtomo, A.; Kawasaki, M. & Koinuma, H. (2000). Optical and photoelectrical properties of oriented ZnO films. *J. Appl. Phys.*, 87, 1844-1849

Spaziani, F.; Rossi, M. C.; Salvatori, S.; Conte, G. & Ascarelli, P. (2003). Optimized spectral collection efficiency obtained in diamond-based ultraviolet detectors using a three-electrode structure. *Appl. Phys. Lett.*, 82, 3785-3788

Lu, Z. Q.; Zhao, K.; Liu, H.; Zhou, N.; Gao, L.; Zhao, S. Q. & Wang, A. J. (2009). Fast lateral photovoltaic effect in ferroelectric $LiNbO_3$ single crystals. *Chin. Opt. Lett.*, 7, 718-719

Li, X. M.; Wang, F.; Zhao, K. & Zhao, S. Q. (2010). Ultraviolet laser-induced photovoltaic effects in miscut ferroelectric $LiNbO_3$ single crystals. *Chin. Phys. B*, 19, 077801

Wemple, S. H.; DiDomenico, M. & Camlibel, I. (1968). Relationship between linear and quadratic electro-optic coefficients in $LiNbO_3$, $LiTaO_3$, and other oxygen-octahedra ferroelectrics based on direct measurement of spontaneous polarization. *Appl. Phys. Lett.*, 12, 209-212

Feng, H. X.; Wen, J. K.; Wang, H. & Wang, H. F. (1990). Studies of absorption spectra and the photovoltaic effect in $LiNbO_3$:Mg:Fe crystals. *Appl. Phys. A*, 51, 394-397

Glass, A. M.; D.von der Linde & Negran, T. J. (1974). High-voltage bulk photovoltaic effect and the photorefractive process in $LiNbO_3$. *Appl. Phys. Lett.*, 25, 233-236

Nakamura, M.; Takekawa, S.; Liu, Y.; Kumaragurubaran, S.; Babu, S. M.; Hatano, H. & Kitamura, K. (2008). Photovoltaic effect and photoconductivity in Sc-doped near-stoichiometric $LiNbO_3$ crystals. *Opt. Mater.*, 31, 280-283

Schirmer, O. F. & Linde, D. von der (1978). Two-photon and x-ray-induced Nb^{4+} and O^- small polarons in $LiNbO_3$. *Appl. Phys. Lett.*, 33, 35-39

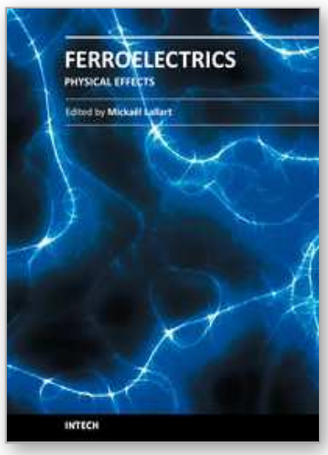

Ferroelectrics - Physical Effects

Edited by Dr. MickaÃ«l Lallart

ISBN 978-953-307-453-5
Hard cover, 654 pages
Publisher InTech
Published online 23, August, 2011
Published in print edition August, 2011

Ferroelectric materials have been and still are widely used in many applications, that have moved from sonar towards breakthrough technologies such as memories or optical devices. This book is a part of a four volume collection (covering material aspects, physical effects, characterization and modeling, and applications) and focuses on the underlying mechanisms of ferroelectric materials, including general ferroelectric effect, piezoelectricity, optical properties, and multiferroic and magnetoelectric devices. The aim of this book is to provide an up-to-date review of recent scientific findings and recent advances in the field of ferroelectric systems, allowing a deep understanding of the physical aspect of ferroelectricity.

InTech Europe
University Campus STeP Ri
Slavka Krautzeka 83/A
51000 Rijeka, Croatia
Phone: +385 (51) 770 447
Fax: +385 (51) 686 166
www.intechopen.com

InTech China
Unit 405, Office Block, Hotel Equatorial Shanghai
No.65, Yan An Road (West), Shanghai, 200040, China
中国上海市延安西路65号上海国际贵都大饭店办公楼405单元
Phone: +86-21-62489820
Fax: +86-21-62489821

IntechOpen